

GPA-Tree: Statistical Approach for Functional-Annotation-Tree-Guided Prioritization of GWAS Results

Aastha Khatiwada¹, Bethany J. Wolf¹, Ayse Selen Yilmaz², Paula S. Ramos^{1, 3}, Maciej Pietrzak², Andrew Lawson¹, Kelly J. Hunt¹, Hang J. Kim⁴, and Dongjun Chung^{2, *}

¹Department of Public Health Sciences, Medical University of South Carolina, Charleston, South Carolina, USA

²Department of Biomedical Informatics, The Ohio State University, Columbus, Ohio, USA

³Department of Medicine, Medical University of South Carolina, Charleston, South Carolina, USA

⁴Division of Statistics and Data Science, University of Cincinnati, Cincinnati, Ohio, USA

*To whom correspondence should be addressed (chung.911@osu.edu).

Abstract

Motivation: In spite of great success of genome-wide association studies (GWAS), multiple challenges still remain. First, complex traits are often associated with many single nucleotide polymorphisms (SNPs), each with small or moderate effect sizes. Second, our understanding of the functional mechanisms through which genetic variants are associated with complex traits is still limited. functional annotations related to risk-associated SNPs. To address these challenges, we propose GPA-Tree and it simultaneously implements association mapping and identifies key combinations of functional annotations related to risk-associated SNPs by combining a decision tree algorithm with a hierarchical modeling framework.

Results: First, we implemented simulation studies to evaluate the proposed GPA-Tree method and compared its performance with existing statistical approaches. The results indicate that GPA-Tree outperforms existing statistical approaches in detecting risk-associated SNPs and identifying the true combinations of functional annotations with high accuracy. Second, we applied GPA-Tree to a systemic lupus erythematosus (SLE) GWAS and functional annotation data including GenoSkyline and GenoSkylinePlus. The results from GPA-Tree highlight the dysregulation of blood immune cells, including but not limited to primary B, memory helper T, regulatory T, neutrophils and CD8⁺ memory T cells in SLE. These results demonstrate that GPA-Tree can be a powerful tool that improves association mapping while facilitating understanding of the underlying genetic architecture of complex traits and potential mechanisms linking risk-associated SNPs with complex traits.

Availability: The GPATree software is available at <https://dongjunchung.github.io/GPATree/>.

1 Introduction

As of February 2021, the genome-wide association studies (GWAS) Catalog has published 4,865 GWAS studies and identified 247,051 genotype-trait associations (<https://www.ebi.ac.uk/gwas/>) [3]. While the number of identified genotype-trait associations has increased substantially in the last decade, there are multiple challenges that still need to be addressed to improve identification of genotype-trait associations and to prioritize the likely causal variants. First, it has been shown that a complex trait can be influenced

by multiple single nucleotide polymorphisms (SNPs), often with small or moderate effect sizes [33, 31]. Such SNPs often do not meet the genome-wide p -value cutoff of 5×10^{-8} and as a result, still many trait-associated SNPs remain unidentified. In theory, utilizing a large sample size will improve statistical power to detect these SNPs. However, traits of limited prevalence in the population often result in limited sample sizes, and recruiting a large sample size requires significant resources and is often not feasible. Therefore, there is a critical need to find alternate ways to increase statistical power to detect SNPs with small and moderate effect sizes.

Second, over 85% of the genetic variants identified by GWAS are located in non-coding regions [15] and it is often difficult to understand their functional roles in the trait etiology. For example, in autoimmune diseases, about 90% of the causal genetic variants lie in non-coding regions, a bulk of which are located in regulatory DNA regions [27, 11]. Utilizing tissue- and cell type-specific functional information can potentially improve our understanding of biological mechanisms through which SNPs may be associated with traits [36]. The general hypothesis is that functional roles relevant to trait-associated SNPs may influence the distribution of these SNPs in the GWAS summary statistics. Therefore, integrating GWAS summary statistics and functional annotation information might not only improve statistical power to detect SNPs, but also identify the mechanisms by which trait-associated SNPs may influence trait [28, 39, 36]. For example, in the case of autoimmune diseases like systemic lupus erythematosus (SLE) and multiple sclerosis (MS), risk-associated SNPs might be more enriched for those with roles in immunity, while for psychiatric disorders like bipolar disorder (BPD) and schizophrenia (SCZ), risk-associated SNPs might be more relevant to the central nervous system or brain function.

Recognizing the potential of such integrative approaches, several methods have been proposed to prioritize SNPs and identify relevant functional annotations by integrating GWAS data with functional annotation data [36, 39, 22, 25, 28, 29]. Still currently available methods utilize functional annotations in a relatively simple form without considering interactions between them, i.e., only main effects terms are included in the model. However, this can be a critical limitation because valuable in-depth biological insight can often be obtained through investigating combinations of the functional annotations, e.g., different types of histone modifications, epigenetic marks in different immune cell subsets, and expression quantitative trait loci (eQTL) for different traits. In theory, some existing methods can be extended by including interaction terms to identify combinations of functional annotations. However, this requires strong prior scientific knowledge, which is often lacking, especially when a large number of functional annotations is considered in the analysis. Moreover, including all possible interactions can quickly become computationally taxing. Therefore, there is a critical need for a method that can efficiently identify relevant combinations of functional annotations without requiring strong prior knowledge.

To fill in this important research gap, we propose GPA-Tree, a novel statistical approach that simultaneously prioritizes trait-associated SNPs and identifies key combinations of functional annotations related to the mechanisms through which trait-associated SNPs influence the trait, within a unified framework. Specifically, GPA-Tree is based on a hierarchical modeling approach integrated with a decision tree algorithm and facilitates easy interpretation of findings. GPA-Tree takes GWAS summary statistics as input, which allows wide applications and adaptations. Our comprehensive simulation studies and real data applications show that GPA-Tree consistently improves statistical power to detect trait-associated SNPs and also effectively identifies biologically important combinations of functional annotations.

2 GPA-Tree

2.1 Model

Let $\mathbf{Y}_{M \times 1} = (Y_1, Y_2, \dots, Y_M)'$ be a vector of genotype-trait association p -values for $i = 1, 2, \dots, M$ such that y_i denotes the p -value for the association of the i^{th} SNP with the trait. We also assume that we have K binary annotations (\mathbf{A}).

$$\mathbf{A} = (\mathbf{A}_{.1}, \dots, \mathbf{A}_{.K}) = \begin{pmatrix} a_{11} & \dots & a_{1K} \\ \vdots & \ddots & \vdots \\ a_{M1} & \dots & a_{MK} \end{pmatrix}_{M \times K}, \text{ where}$$

$$a_{ik} = \begin{cases} 0, & \text{if } i^{th} \text{ SNP is not annotated in the } k^{th} \text{ annotation} \\ 1, & \text{if } i^{th} \text{ SNP is annotated in the } k^{th} \text{ annotation} \end{cases}$$

Here our ultimate goal is association mapping, i.e., identifying SNPs associated with the trait given both GWAS and functional annotation data. To accomplish this, we introduce the latent variable \mathbf{Z} , where z_i indicates association of i^{th} SNP with the trait. Then, the GWAS association p -values (y_i) are assumed to come from a mixture of non-risk-associated ($z_i = 0$) and risk-associated groups ($z_i = 1$). As previously proposed by Chung and colleagues [7], if the i^{th} SNP belongs to the non-risk-associated group ($z_i = 0$), then its p -value is assumed to come from the Uniform distribution on $[0, 1]$. This is based on the rationale that $U[0, 1]$ provides a p -value density corresponding to the non-risk-associated group [32]. If the i^{th} SNP belongs to the risk-associated group ($z_i = 1$), then its p -value is assumed to come from the Beta distribution with parameters $(\alpha, 1)$, where $0 < \alpha < 1$. We restrict α in the Beta distribution to be between 0 and 1 because the smaller α value corresponds to the higher density at lower p -values, while the α value closer to one resembles a $Unif[0, 1]$ distribution.

We further integrate functional annotation data with the GWAS data by modeling the latent \mathbf{Z} as a function of the functional annotation data \mathbf{A} . Specifically, we define a function f that is a combination of functional annotations \mathbf{A} and relate it to the expectation of latent \mathbf{Z} as given in Equation (1).

$$P(Z_i = 1; a_{i1}, \dots, a_{iK}) = f(a_{i1}, \dots, a_{iK}) \tag{1}$$

Let $\theta = (\alpha, \boldsymbol{\pi})$, where $\boldsymbol{\pi} = \{\pi_1, \pi_2, \dots, \pi_M\}$ is a function of \mathbf{A} and represents the prior probabilities that the SNPs belong to the risk-associated group, i.e., $\pi_i = P(Z_i = 1)$. See Section 1 in the Supplementary Materials for the joint distribution of the observed data, and the incomplete and complete data log-likelihoods.

2.2 Algorithm

Given the approach described in Section 2.1, we implemented parameter estimation using an EM algorithm. The function f in Equation (1) is estimated by a decision tree algorithm and it allows to identify combinations of functional annotations related to risk-associated SNPs. To improve stability, we employed a two-stage approach for parameter estimation. Specifically, in Stage 1, we first estimate the parameter α without identifying a combination of functional annotations. Then, in Stage 2, we identify key combinations of functional annotations ($f(\mathbf{A})$) while the parameter α is kept fixed as the value obtained in the first step. We illustrate more detailed calculation steps below.

Stage 1:

For the i^{th} SNP, the t^{th} iteration of the E-step can be written as:

$$\begin{aligned}
\mathbf{E} - \mathbf{step} : \mathbf{z}_i^{(t)} &= \mathbf{E}[\mathbf{Z}_i; \mathbf{Y}, \mathbf{A}, \boldsymbol{\theta}^{(t-1)}] \\
&= Pr(Z_i = 1; \mathbf{Y}, \mathbf{A}, \boldsymbol{\theta}^{(t-1)}) \\
&= \frac{P(Y_i; Z_i=1, \boldsymbol{\theta}^{(t-1)})P(Z_i=1; \mathbf{A}_{i\cdot}, \boldsymbol{\theta}^{(t-1)})}{\sum_{d \in \{1,0\}} P(Y_i; Z_i=d, \boldsymbol{\theta}^{(t-1)})P(Z_i=d; \mathbf{A}_{i\cdot}, \boldsymbol{\theta}^{(t-1)})} \\
&= \frac{\alpha^{(t-1)} y_i^{\alpha^{(t-1)} - 1} \pi_i^{(t-1)}}{1 - \pi_i^{(t-1)} + \alpha^{(t-1)} y_i^{\alpha^{(t-1)} - 1} \pi_i^{(t-1)}}
\end{aligned} \tag{2}$$

In the t^{th} iteration of the M-step, π_i and α are updated as:

$$\begin{aligned}
\mathbf{M} - \mathbf{step} : & \text{Fit a linear regression model as} \\
z_i^{(t)} &= \beta_0^{(t)} + \beta_1^{(t)} a_{i1} + \dots + \beta_K^{(t)} a_{iK} + \epsilon_i^{(t)} \\
& \text{Update } \pi_i^{(t)} \text{ as the predicted value from the linear regression model.} \\
& \text{Update } \alpha^{(t)} = - \sum_{i=1}^M z_i^{(t)} / \sum_{i=1}^M z_i^{(t)} \log(y_i),
\end{aligned} \tag{3}$$

where $\beta_k^{(t)}$, $k = 0, \dots, K$ are the regression coefficients and $\epsilon_i^{(t)}$ is the error term. The E and M steps are repeated until both the incomplete log-likelihood and the α estimate converge. The α and $\boldsymbol{\pi}$ estimated in this stage are used to fix α and initialize $\boldsymbol{\pi}$, respectively, in Stage 2.

Stage 2:

In this stage, we implement another EM algorithm employing a decision tree algorithm (CART [2]), which allows to identify union, intersection, and complement relationships between functional annotations in estimating π_i .

For the i^{th} SNP, the t^{th} iteration of the E-step can be written as:

$$\mathbf{E} - \mathbf{step} : z_i^{(t)} = \frac{\hat{\alpha} y_i^{\hat{\alpha} - 1} \pi_i^{(t-1)}}{1 - \pi_i^{(t-1)} + \hat{\alpha} y_i^{\hat{\alpha} - 1} \pi_i^{(t-1)}} \tag{4}$$

Note that here α is fixed as $\hat{\alpha}$, which is the final estimate of α obtained from Stage 1. In the t^{th} iteration of the M-step, π_i is updated as:

$$\begin{aligned}
\mathbf{M} - \mathbf{step} : & \text{Fit a CART model as} \\
z_i^{(t)} &= f^{(t)}(a_{i1}, \dots, a_{iK}) + \epsilon_i^{(t)} \\
& \text{Update } \pi_i^{(t)} \text{ as the predicted value from the CART model,}
\end{aligned} \tag{5}$$

where ϵ_i is the error term. In the M-step, the complexity parameter (cp) is the key tuning parameter and defined as the minimum improvement that is required at each node of the tree. Specifically, in the CART model, the largest possible tree (i.e., a full-sized tree) is first constructed and then pruned using cp . The pruned regression tree structure identified by the CART model upon convergence of the EM algorithm (Equation (5)) is used as f in Equation (1). This approach allows for the construction of the accurate yet interpretable regression tree that can explain relationships between functional annotations and genotype-trait associations. The E and M steps are repeated until the incomplete log-likelihood converges.

We note that unlike the standard EM algorithm, the incomplete log-likelihood in Stage 2 is not guaranteed to be monotonically increasing. Therefore, we implement Stage 2 as a generalized EM algorithm by retaining only the iterations in which the incomplete log-likelihood increases compared to the previous iteration.

2.3 Prioritization of risk-associated SNPs and identification of relevant combinations of functional annotations

Once the parameters are estimated as described in Section 2.2, we can now prioritize risk-associated SNPs and identify combinations of functional annotations relevant to these SNPs. First, SNPs are prioritized using the local false discovery rate, fdr , which is defined as the posterior probability that the i^{th} SNP belongs to the non-risk-associated group given its GWAS p -value and functional annotation information, i.e., $fdr(Y_i, \mathbf{A}_i) = P(Z_i = 0; Y_i, \mathbf{A}_i) = 1 - P(Z_i = 1; Y_i, \mathbf{A}_i)$. We utilize the ‘direct posterior probability’ approach [30] to control the global false discovery rate, FDR , which is the expected ratio of the number of SNPs that are incorrectly predicted to be risk-associated SNPs (false positives) compared to the number of SNPs that are predicted to be risk-associated SNPs (positives). In this approach, SNPs are first sorted by their fdr in an ascending order, denoted as h_i . The threshold for fdr , κ , is then increased from 0 to 1 until

$$FDR = \frac{\sum_{i=1}^M h_i 1\{h_i \leq \kappa\}}{\sum_{i=1}^M 1\{h_i \leq \kappa\}} \leq \tau,$$

where τ is the predetermined level of FDR (e.g., $\tau \leq 0.05$). Finally, SNPs with $h_i \leq \kappa$ are considered to be risk-associated SNPs. Second, relevant combinations of annotations are inferred based on the combination of functional annotations selected by the CART model upon convergence of the EM algorithm in Stage 2.

2.4 ShinyGPATree: Shiny app for interactive analysis of risk-associated SNPs and the functional annotation tree

We implemented the forementioned GPA-Tree algorithm as an R package ‘GPATree’. To further facilitate user’s convenience, we developed ‘ShinyGPATree’, a Shiny app for interactive analysis of risk-associated SNPs and the functional annotation tree (Fig 1). This Shiny app can be open by sequentially running `GPATree()` and `ShinyGPATree()` functions. First, the `GPATree()` function takes 4 arguments: `gwasPval`, `annMat`, `initAlpha` and `cpTry`. `gwasPval` is a $M \times 1$ matrix of GWAS association p -values for M SNPs, `annMat` is a $M \times K$ matrix of K binary functional annotations for M SNPs, `initAlpha` is the initial alpha value to be used to fit the GPA-Tree model (default value = 0.1), and `cpTry` is the cp parameter to be used to fit the GPA-Tree model (default value = 0.001). The `GPATree()` function generates a GPA-Tree model fit required for the ShinyGPATree app. The `ShinyGPATree()` function takes the output of `GPATree()` as an input and opens the ShinyGPATree app using the R code below.

```
R> fit <- GPATree(gwasPval, annMat, initAlpha, cpTry)
R> ShinyGPATree(fit)
```

The ShinyGPATree app provides visualization of the GPA-Tree model fit, identifies risk-associated SNPs, and characterizes the combinations of functional annotations that can describe the risk-associated SNPs. The app also allows to improve the visualization of the GPA-Tree model fit by collating or separating layers of the model using the cp parameter. The number of non-risk-associated and risk-associated SNPs that can be characterized by combinations of functional annotations are also automatically updated based on user-selected cp , FDR type (global vs. local) and FDR level values. The interactive nature of the app allows users to effortlessly interact with the GPA-Tree model results to generate plots, prioritize risk SNPs, and make inferences about relevant combinations of functional annotations for the risk-associated SNPs. ShinyGPATree consists of two main tabs, namely ‘Plot’ and ‘Info’, which are explained in detail below.

ShinyGPATree

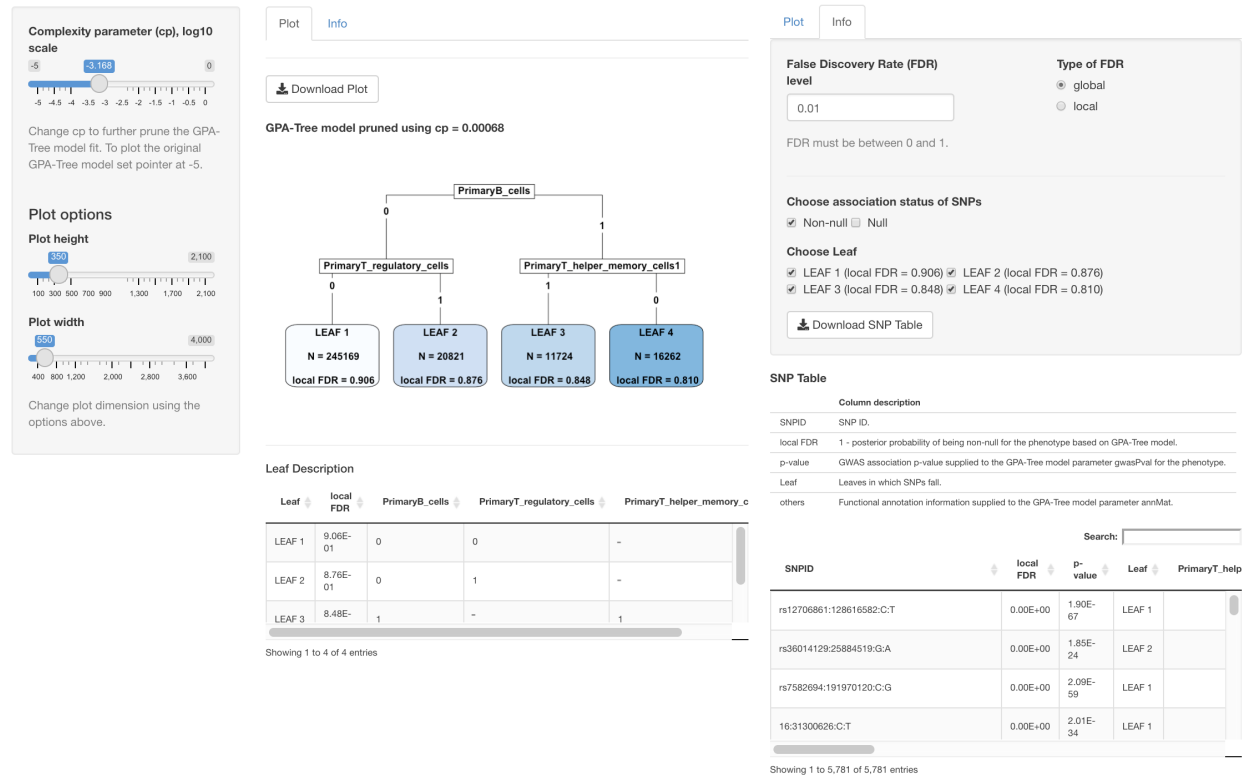


Figure 1: Screenshot of the ShinyGPATree app with (A) the ‘Plot’ tab and (B) the ‘Info’ tab open.

2.4.1 Plot tab: Visualization of the GPA-Tree model

Fig 1A shows the layout of the ShinyGPATree app, where the ‘Plot’ tab opens by default. In the displayed plot, each leaf (terminal node) is characterized by combinations of the functional annotations that are encountered as users move from the root node to the leaf. The summary information is provided for each leaf, including the number of SNPs that satisfy the combination of functional annotations specific to the leaf and the mean local FDR for these SNPs. The summary information displayed in each leaf is automatically updated as the user modifies the *cp* value on the left panel. Users can also improve visualization of the functional annotation tree plot using the *Plot width* and *Plot height* options on the left panel. The ‘Download Plot’ button on the top allows users to download the functional annotation tree plot as a PNG format file. Finally, a table titled ‘Leaf Description’ underneath the plot characterizes the functional annotations that are 0 or 1 for SNPs in specific leaves.

2.4.2 Info tab: Association mapping and annotation selection

The ‘Info’ tab opens the user interface for association mapping and functional annotation characterization for SNPs as seen in Fig 1B. Under this tab, users can find more information on specific SNPs driving the visualization. The top of the panel provides multiple options to control association mapping, including FDR level and FDR type (global vs. local). It also provides options to select which SNPs to display, e.g., choosing SNPs that fall on specific leaves of the GPA-Tree model and/or selecting SNPs with specific association status (non-risk-associated vs. risk-associated SNPs). The ‘SNP Table’ at the bottom of the ‘Info’ tab panel shows information about the SNPs that satisfy these options. Each row of the table represents a SNP, where columns include SNP ID, local FDR value, GWAS association *p*-value, the leaf

ID in which the SNP is located, and the corresponding complete functional annotation information. The ‘Download SNP Table’ button allows users to download the ‘SNP Table’ as a CSV format file.

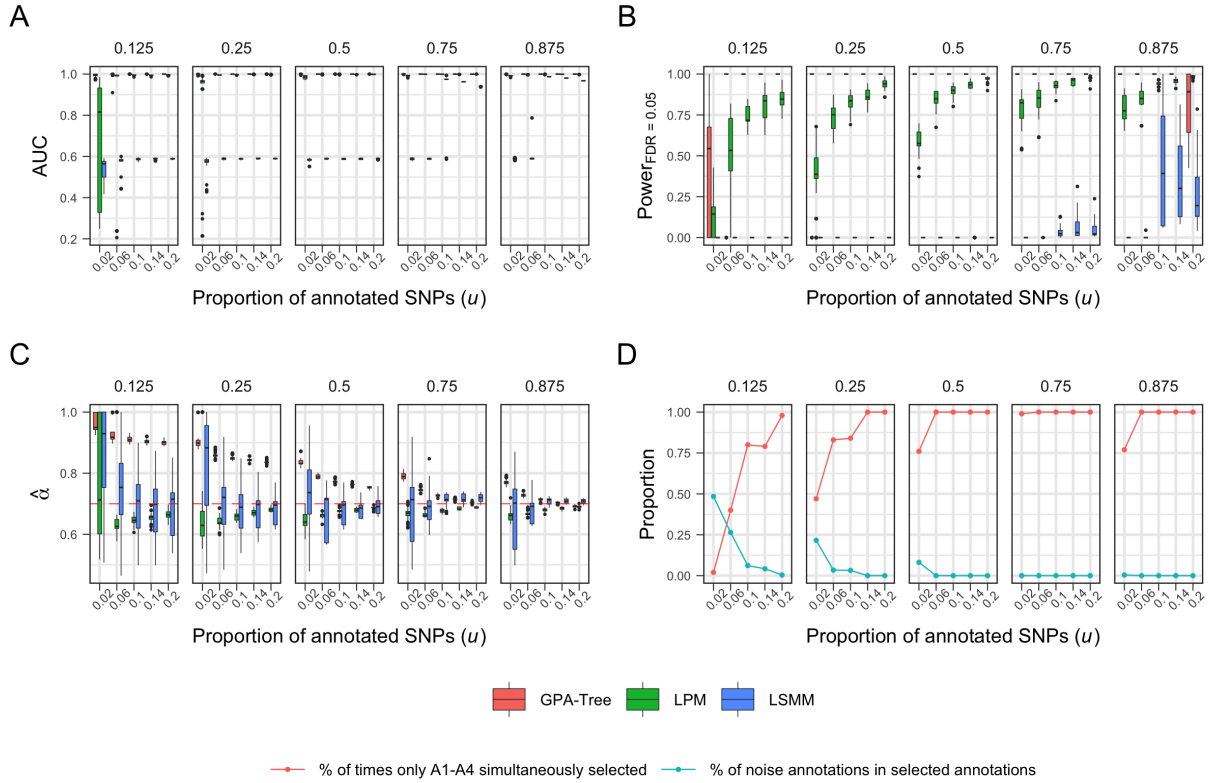


Figure 2: Comparison of (A) AUC, (B) statistical power to detect true risk-associated SNPs when global FDR is controlled at the nominal level of 0.05, (C) estimated α parameter, and (D) proportion of times only true functional annotations $A_1 - A_4$ are simultaneously identified by GPA-Tree (red line) and the average proportion of noise annotations ($A_5 - A_{75}$) among the functional annotations identified by GPA-Tree (blue line). The results are presented for different proportions of SNPs annotated in $A_1 - A_4$ (u ; x-axis) and proportions of the overlap between SNPs annotated in $A_1 - A_2$ and $A_3 - A_4$ (v ; panel). $M = 100,000$, $K = 75$, and $\alpha = 0.7$ in $Beta(\alpha, 1)$ and results are summarized from 100 replications.

3 Results

3.1 Simulation study

We conducted a simulation study to evaluate the performance of the proposed GPA-Tree approach. For all the simulation data, the number of SNPs was set to $M = 100,000$, the number of annotations was set to $K = 75$, and risk-associated SNPs were assumed to be characterized with the combinations of functional annotations defined by $L = (A_1 \cap A_2) \cup (A_3 \cap A_4)$; all the remaining functional annotations ($A_k, k = 5, \dots, 75$) were considered to be noise annotations. The percentage of annotated SNPs (u) for annotations $A_1 - A_4$ was set to 2%, 6%, 10%, 14% and 20%, while the percentage of overlap between the true combinations of functional annotations (v) was set to 12.5%, 25%, 50%, 75% and 87.5%. For noise annotations $A_5 - A_{75}$, approximately 20% of SNPs were annotated by first generating the proportion of annotated SNPs from $Unif[0.1, 0.3]$ and then randomly setting this proportion of SNPs to one. The

SNPs that satisfy the functional annotation combination L were assumed to be risk-associated SNPs and their p -values were simulated from $Beta(\alpha, 1)$ with $\alpha = 0.7$. The SNPs that do not satisfy L were assumed to be non-risk SNPs and their p -values were simulated from $U[0, 1]$.

For each combination of the simulation parameters defined above, we simulated 100 datasets and compared the performance of GPA-Tree with LPM [29] and LSMM [28]. The metrics for comparing the methods include (1) area under the curve (AUC), where the curve was created by plotting the true positive rate (sensitivity) against the false positive rate (1-specificity) to detect risk-associated SNPs when global FDR was controlled at various levels; (2) statistical power to identify risk-associated SNPs when global FDR was controlled at the nominal level of 0.05; and (3) estimation accuracy for α parameter in the $Beta(\alpha, 1)$ distribution used to generate the p -values of risk-associated group. For GPA-Tree, we also examined the accuracy of detecting the correct functional annotation tree, based on the proportion of simulation data for which all relevant functional annotations in L ($A_1 - A_4$) were identified simultaneously, and the average proportion of noise functional annotations ($A_5 - A_{75}$) among the functional annotations identified by GPA-Tree. Here we especially investigate how the percentage of SNPs annotated in $A_1 - A_4$ (u) and the overlap between SNPs annotated in $A_1 - A_2$ and $A_3 - A_4$ (v) impact GPA-Tree’s ability to separate functional annotations relevant to the risk-associated SNPs from noise annotations.

- **AUC:** Fig 2A shows the AUC comparison between GPA-Tree, LPM, and LSMM. For all the combinations of u and v , GPA-Tree showed the consistently higher AUC relative to LSMM while performing comparably or better than LPM. The performance of LPM and LSMM improved as signal-to-noise ratio increases (i.e., as u and v increase), demonstrating performance closer to GPA-Tree.
- **Statistical power:** Fig 2B compares the power to detect true risk-associated SNPs when global FDR is controlled at 0.05 for the three methods. GPA-Tree showed higher statistical power to detect true risk-associated SNPs relative to LPM and LSMM for almost all combinations of u and v . The estimated power for GPA-Tree was relatively more variable for $u = 2\%$ and $v = 12.5\%$ but it still outperformed LPM and LSMM. The statistical power of LPM increased as a function of u for all v , and the statistical power of LSMM increased as u increases for higher v . However, both LPM and LSMM showed greater variability in statistical power compared to GPA-Tree and on average they showed lower statistical power compared to GPA-Tree.
- **Estimation of parameter α :** Fig 2C shows the α parameter estimates obtained from the three methods. GPA-Tree showed less variability in the α estimates compared to LPM and LSMM. LPM was on average more accurate than GPA-Tree in estimating α , however it still often underestimated α . LSMM showed decreased variability in estimation of α as u increases, and estimated α well for higher u and v levels. GPA-Tree generally overestimated α and this was most notable when u and v are small. As u and v increase, α estimates from GPA-Tree became closer to the true value. When u and v are large ($u \geq 10\%$ and $v \geq 75\%$), GPA-Tree estimated α accurately. We note that overestimation of α by GPA-Tree did not impact the method’s ability to identify the true combinations of functional annotations or the risk-associated SNPs, which are the main objectives of GPA-Tree.
- **Selection of relevant and noise annotations:** The red line in Fig 2D shows the proportion of times only functional annotations in the true combination L ($A_1 - A_4$) were simultaneously identified by GPA-Tree while the blue line shows the proportion of noise annotations ($A_5 - A_{75}$) that were also selected. Excluding instances when signal in the data is really weak ($u \leq 6\%$ and $v \leq 25\%$), GPA-Tree successfully identified all functional annotations included in the true combination L more than 75% of the time. Moreover, GPA-Tree could identify all functional annotations included in the true combination approximately 100% of the time as u or v get larger (Fig 2D, red line). These

results demonstrate the potential of GPA-Tree to correctly identify true annotations as long as signal in the data is not too weak. In instances where GPA-Tree did not identify all functional annotations included in L , it either identified one or more noise annotations in addition to the true annotations (false positives), or failed to identify one or more annotations in L (false negative) (Fig 2D, blue line).

3.2 Real data analysis

We applied the GPA-Tree approach to the SLE GWAS data [20] sourced from the GWAS Catalog [3] (<https://www.ebi.ac.uk/gwas/>). Summary statistics were originally obtained using the genotyped and imputed ImmunoChip, profiled for 18,264 individuals (6,748 cases and 11,516 controls) of European ancestry. 336,745 SNPs passed quality control criteria. After excluding SNPs located in the MHC region, 293,976 SNPs were included in the final analysis and integrated with functional annotation data from GenoSkyline (GS) [24] and GenoSkylinePlus (GSP) [23]. GS were generated by integrating epigenetic annotations from the Roadmap Epigenomics Consortium [19]. They predict tissue-specific functional relevance for SNPs, which are available for seven tissue clusters (brain, gastrointestinal/GI, lung, heart, blood, muscle and epithelium tissues). GSP added another layer of information to GS in the form of epigenomic and transcriptomic annotations, and are available for 127 annotation tracks. The Manhattan plot and p -value histogram for SLE GWAS data are presented in Fig S1 in the Supplementary Materials.

3.2.1 Tissue-level investigation

We initially investigated the functional potential of all SNPs using seven tissue-specific GS annotations. With a GS score cutoff of 0.5, 35.90% of SNPs were annotated in at least one of the seven tissue types (Fig S2A in the Supplementary Materials) and the percentage of annotated SNPs ranged from 8.66% for lung tissue to 19.14% for blood tissue (Fig S2B in the Supplementary Materials). We also measured the overlap in SNPs annotated in different tissue types using log odds ratio (Fig S2C in the Supplementary Materials). While the highest proportion of SNPs is annotated for blood tissue, SNPs annotated for blood tissue overlap less with other tissue types. On the contrary, SNPs annotated for heart, lung and muscle tissues overlap more with other tissue types. This is consistent with the literature indicating that blood shows the lowest levels of eQTL sharing with other tissue types while muscle and lung tissues show higher levels of eQTL sharing [38, 24]. Next, we applied GPA-Tree to the SLE GWAS and GS annotation data for association mapping and characterization of relevant functional annotations. GPA-Tree identified 8,962 SLE-associated SNPs at the nominal global FDR level of 0.05. Among SLE-associated SNPs, 46.40% were annotated for at least one of the seven GS tissue type (Fig S3A in the Supplementary Materials), and the percentage of annotated SNPs ranged from 9.89% for lung tissue to 30.22% for blood tissue (Fig S3B in the Supplementary Materials). We also measured relative enrichment (RE), the ratio of the proportion of SLE-associated SNPs annotated for a specific tissue type, relative to the proportion of non-SLE-associated SNPs annotated for the same tissue type. RE was again highest for the blood tissue with the value of 1.61 (Fig S3C in the Supplementary Materials). These results are consistent with the dysregulation of blood immune cells that characterizes SLE and other autoimmune diseases like Crohn’s disease, ulcerative colitis and rheumatoid arthritis [24].

The original GPA-Tree model fit contained blood tissue at the root node and included 28 leaves. For easier interpretation, we used ShinyGPATree app to prune the tree so that it includes 7 leaf nodes (Fig 3A). We note that although it is occasionally possible to obtain a large functional annotation tree that can be cumbersome to visualize and interpret, the ShinyGPATree app can be utilized to manage such cases as it allows users to investigate different layers of functional annotation trees in an interactive and dynamic manner. For example, the annotation combination for SNPs in leaf 7 can be written as Blood

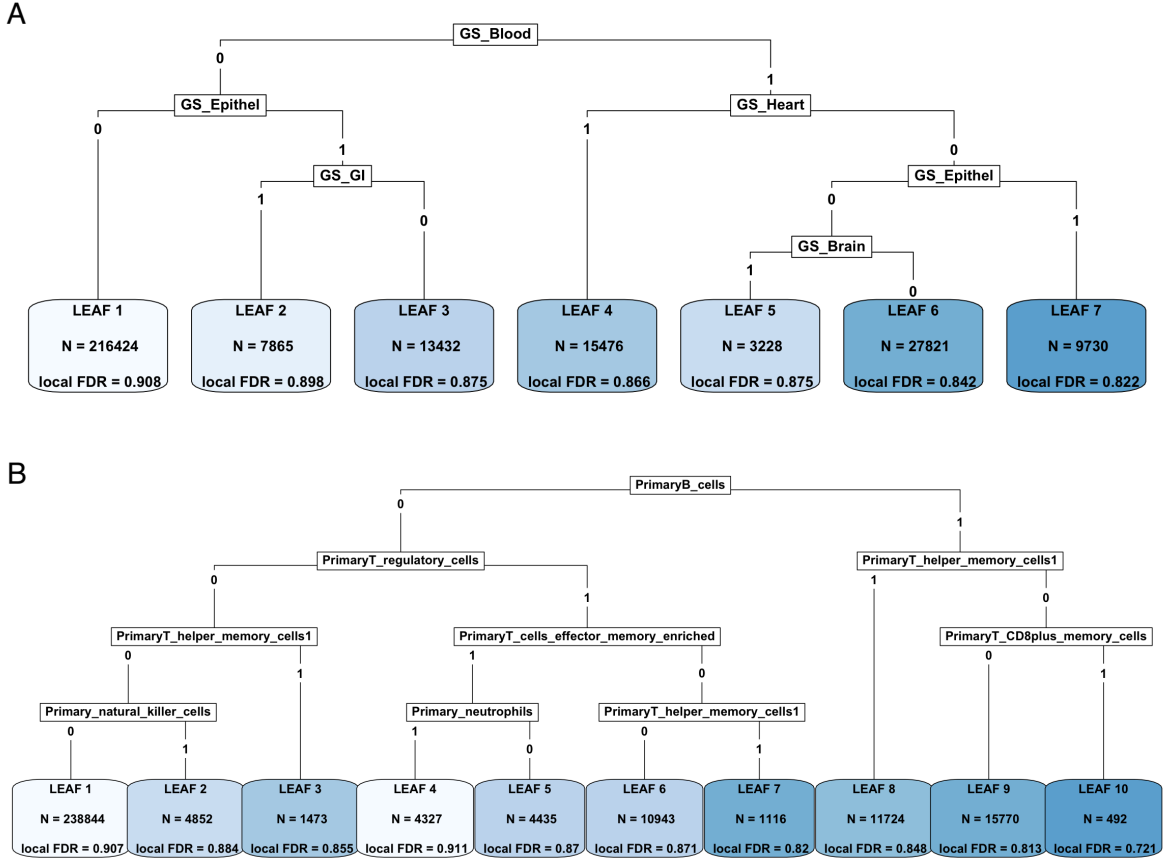


Figure 3: Functional annotation tree identified by GPA-Tree approach when (A) seven tissue-level GenoSkyline (GS) annotations and (B) 10 blood-related cell-type-level GenoSkylinePlus (GSP) annotations are considered. Both trees were generated by pruning the GPA-Tree model fit using $cp = 2.5 \times 10^{-4}$. Each leaf (terminal node) in the tree shows the total number of SNPs in the leaf and the mean local FDR for the SNPs in the leaf.

\cap !Heart \cap Epithelium, i.e., leaf 7 includes SNPs that are annotated for blood and epithelium tissues but not for heart tissue. The number of SNPs that are located in each leaf node, and the combination of functional annotations that describe SNPs in each leaf node are displayed in Fig 3A. Further investigation of the GPA-Tree model fitting results showed that, among the 8,962 SLE-associated SNPs, 578 are concurrently annotated for blood and epithelium tissues while not being annotated for heart tissue as represented in leaf 7; 609 are concurrently annotated for both blood and heart tissues as represented in leaf 4; and 230 are concurrently annotated for epithelium and GI tissues while not being annotated for blood tissue as represented in leaf 2. Blood, epithelium, GI and heart also have the largest RE (Fig S3C in the Supplementary Materials). In general, our results are consistent with the literature indicating relevance of blood tissue in SLE, and further add genomic-level support to the relevance of other tissues concurrently with blood [5, 13, 16, 10].

3.2.2 Cell-type-level investigation

Based on the observed relationship between GS annotation for blood tissue and SLE, in the second phase of the real data analysis, we considered 10 blood-related GSP functional annotations. With a GSP

score cutoff of 0.5, 25.29% were annotated in at least one of the 10 GSP blood annotations (Fig S4A in the Supplementary Materials) and the highest enrichment was observed for primary regulatory T cells (12.13%) (Fig S4B in the Supplementary Materials). The highest overlaps were observed between SNPs annotated with primary memory helper T, effector memory T and CD8⁺ memory T cells (Fig S4C in the Supplementary Materials).

Next, we applied GPA-Tree to the SLE GWAS and GSP blood annotations. At the nominal global FDR level of 0.05, GPA-Tree identified 8,993 SLE-associated SNPs, where 8,723 among those overlapped with the SNPs prioritized in the first phase using GS annotations. Among the SLE-associated SNPs prioritized in the second phase, 37.54% were annotated for at least one of the 10 GSP blood annotations (Fig S5A in the Supplementary Materials). The largest proportion of SLE-associated SNPs was annotated for primary B cells (19.47%), followed by primary regulatory T cells (18.45%) (Fig S5B in the Supplementary Materials). Primary B cells also showed the highest RE with the value of 2.12 (Fig S5C in the Supplementary Materials). Since SLE is characterized by the production of autoantibodies, the involvement of B cells, which produce antibodies, is consistent with disease pathology.

The original GPA-Tree model with GSP blood annotations identified primary B cells at the root node and included 172 leaves. Again, to improve interpretability and visualization, we used ShinyGPATree to prune the tree so that it includes 10 leaf nodes (Fig 3B). In addition to primary B cells, other blood-related GSP functional annotations identified as important included primary memory helper T, regulatory T, neutrophils, natural killer, effector memory T, and CD8⁺ memory T cells. Among the 8,993 SLE-associated SNPs, 613 are concurrently annotated for primary B and helper memory T cells as represented in leaf 8; 68 are concurrently annotated for primary B and CD8⁺ memory T cells while not being annotated for memory helper T cells as represented in leaf 10; and 108 are concurrently annotated for primary regulatory T, neutrophils and effector memory T cells while not being annotated for primary B cells as represented in leaf 4. Overall, these results are consistent with previous literature indicating connections between SLE and B cells, regulatory T cells, neutrophils and CD8⁺ memory T cells [8, 35, 17, 1, 12].

These results also provide several new insights for future investigations. For instance, among the SLE-associated SNPs, 43 SNPs located in the *CLEC16A* gene and 41 SNPs located in the *IKZF3* gene are in leaf 8 and concurrently regulate primary B and memory helper T cells; however, an additional 16 SNPs in the *CLEC16A* gene are in leaf 4 and concurrently regulate primary regulatory T, neutrophils and effector memory T cells while not regulating B cells. These results provide further evidence that multiple independent SNPs in the same gene locus can have different effects on the levels of different immune cell subtypes [34], and can be utilized to investigate a variant’s functional role in previously defined associations between SLE, *CLEC16A* and *IKZF3* [37, 9, 14, 21, 26, 4], among others.

4 Conclusion

In this paper, we presented GPA-Tree, a novel statistical methodology that integrates GWAS summary statistics and functional annotation data within a unified framework. GPA-Tree simultaneously identifies risk-associated SNPs and combinations of functional annotations that potentially explain the mechanisms through which risk-associated SNPs are related with traits. GPA-Tree showed the higher AUC and statistical power to detect risk-associated SNPs compared to existing approaches. GPA-Tree also successfully identified the true combinations of functional annotations in most cases, facilitating understanding of potential biological mechanisms linking risk-associated SNPs with complex traits. The proposed GPA-Tree approach was implemented as the R package ‘GPATree’ and we also developed ‘ShinyGPATree’, a Shiny app for interactive and dynamic investigation of association mapping results and functional annotation trees. In the future, we plan to further improve the proposed GPA-Tree method to jointly analyze GWAS

data for multiple traits [18, 6]. Overall, the ability of GPA-Tree to improve SNP prioritization and attribute functional characteristics to risk-associated SNPs or gene locus can be powerful in facilitating our understanding of genetic susceptibility factors related to complex traits.

Funding

This work was supported in part by NIH/NIGMS grant R01-GM122078, NIH/NCI grant R21-CA209848, NIH/NIDA grant U01-DA045300, and NIH/NIAMS grants P30-AR072582 and R01-AR071947.

Conflict of Interest: None declared.

References

- [1] Patrick Blanco, Vincent Pitard, Jean-François Viallard, Jean-Luc Taupin, Jean-Luc Pellegrin, and Jean-François Moreau. Increase in activated CD8+ T lymphocytes expressing perforin and granzyme B correlates with disease activity in patients with systemic lupus erythematosus. *Arthritis & Rheumatism: Official Journal of the American College of Rheumatology*, 52(1):201–211, 2005.
- [2] Leo Breiman, Jerome Friedman, Charles J Stone, and Richard A Olshen. *Classification and regression trees*. CRC press, 1984.
- [3] Annalisa Buniello, Jacqueline A L MacArthur, Maria Cerezo, Laura W Harris, James Hayhurst, Cinzia Malangone, Aoife McMahon, Joannella Morales, Edward Mountjoy, Elliot Sollis, et al. The NHGRI-EBI GWAS Catalog of published genome-wide association studies, targeted arrays and summary statistics 2019. *Nucleic acids research*, 47(D1):D1005–D1012, 2019.
- [4] Xinze Cai, Ying Qiao, Cheng Diao, Xiaoxue Xu, Yang Chen, Shuyan Du, Xudong Liu, Nan Liu, Shuang Yu, Dong Chen, et al. Association between polymorphisms of the IKZF3 gene and systemic lupus erythematosus in a Chinese Han population. *PLoS one*, 9(10):e108661, 2014.
- [5] Giuseppe Castellano, Cesira Cafiero, Chiara Divella, Fabio Sallustio, Margherita Gigante, Paola Pontrelli, Giuseppe De Palma, Michele Rossini, Giuseppe Grandaliano, and Loreto Gesualdo. Local synthesis of interferon-alpha in lupus nephritis is associated with type I interferons signature and LMP7 induction in renal tubular epithelial cells. *Arthritis research & therapy*, 17(1):1–13, 2015.
- [6] Dongjun Chung, Hang J Kim, and Hongyu Zhao. graph-GPA: a graphical model for prioritizing GWAS results and investigating pleiotropic architecture. *PLoS computational biology*, 13(2):e1005388, 2017.
- [7] Dongjun Chung, Can Yang, Cong Li, Joel Gelernter, and Hongyu Zhao. GPA: a statistical approach to prioritizing GWAS results by integrating pleiotropy and annotation. *PLoS Genet*, 10(11):e1004787, 2014.
- [8] Denis Comte, Maria P Karampetsou, and George C Tsokos. T cells as a therapeutic target in SLE. *Lupus*, 24(4-5):351–363, 2015.
- [9] Yong Cui, Yujun Sheng, and Xuejun Zhang. Genetic susceptibility to SLE: recent progress from GWAS. *Journal of autoimmunity*, 41:25–33, 2013.
- [10] Ellen C Ebert and Klaus D Hagspiel. Gastrointestinal and hepatic manifestations of systemic lupus erythematosus. *Journal of clinical gastroenterology*, 45(5):436–441, 2011.
- [11] Kyle Kai-How Farh, Alexander Marson, Jiang Zhu, Markus Kleinewietfeld, William J Housley, Samantha Beik, Noam Shores, Holly Whitton, Russell JH Ryan, Alexander A Shishkin, et al. Genetic and epigenetic fine mapping of causal autoimmune disease variants. *Nature*, 518(7539):337–343, 2015.

- [12] Gilberto Filaci, Sabrina Bacilieri, Marco Fravega, Monia Monetti, Paola Contini, Massimo Ghio, Maurizio Setti, Francesco Puppo, and Francesco Indiveri. Impairment of CD8+ T suppressor cell function in patients with active systemic lupus erythematosus. *The Journal of Immunology*, 166(10):6452–6457, 2001.
- [13] Keishi Fujio, Yusuke Takeshima, Masahiro Nakano, and Yukiko Iwasaki. Transcriptome and transomics analysis of systemic lupus erythematosus. *Inflammation and regeneration*, 40(1):1–6, 2020.
- [14] Vesela Gateva, Johanna K Sandling, Geoff Hom, Kimberly E Taylor, Sharon A Chung, Xin Sun, Ward Ortmann, Roman Kosoy, Ricardo C Ferreira, Gunnel Nordmark, et al. A large-scale replication study identifies TNIP1, PRDM1, JAZF1, UHRF1BP1 and IL10 as risk loci for systemic lupus erythematosus. *Nature genetics*, 41(11):1228–1233, 2009.
- [15] Hector Giral, Ulf Landmesser, and Adelheid Kratzer. Into the wild: GWAS exploration of non-coding RNAs. *Frontiers in cardiovascular medicine*, 5:181, 2018.
- [16] Bruce I Hoffman and Warren A Katz. The gastrointestinal manifestations of systemic lupus erythematosus: a review of the literature. In *Seminars in arthritis and rheumatism*, pp. 237–247. Elsevier, 1980.
- [17] Mariana J Kaplan. Neutrophils in the pathogenesis and manifestations of SLE. *Nature Reviews Rheumatology*, 7(12):691–699, 2011.
- [18] Hang J Kim, Zhenning Yu, Andrew Lawson, Hongyu Zhao, and Dongjun Chung. Improving SNP prioritization and pleiotropic architecture estimation by incorporating prior knowledge using graph-GPA. *Bioinformatics*, 34(12):2139–2141, 2018.
- [19] Anshul Kundaje, Wouter Meuleman, Jason Ernst, Misha Bilenky, Angela Yen, Alireza Heravi-Moussavi, Pouya Kheradpour, Zhizhuo Zhang, Jianrong Wang, Michael J Ziller, et al. Integrative analysis of 111 reference human epigenomes. *Nature*, 518(7539):317–330, 2015.
- [20] Carl D Langefeld, Hannah C Ainsworth, Deborah S Cunninghame Graham, Jennifer A Kelly, Mary E Comeau, Miranda C Marion, Timothy D Howard, Paula S Ramos, Jennifer A Croker, David L Morris, et al. Transancestral mapping and genetic load in systemic lupus erythematosus. *Nature communications*, 8(1):1–18, 2017.
- [21] Christopher J Lessard, Indra Adrianto, John A Ice, Graham B Wiley, Jennifer A Kelly, Stuart B Glenn, Adam J Adler, He Li, Astrid Rasmussen, Adrienne H Williams, et al. Identification of IRF8, TMEM39A, and IKZF3-ZPBP2 as susceptibility loci for systemic lupus erythematosus in a large-scale multiracial replication study. *The American Journal of Human Genetics*, 90(4):648–660, 2012.
- [22] Qiongshi Lu, Yiming Hu, Jiehuan Sun, Yuwei Cheng, Kei-Hoi Cheung, and Hongyu Zhao. A statistical framework to predict functional non-coding regions in the human genome through integrated analysis of annotation data. *Scientific reports*, 5:10576, 2015.
- [23] Qiongshi Lu, Ryan L Powles, Sarah Abdallah, Derek Ou, Qian Wang, Yiming Hu, Yisi Lu, Wei Liu, Boyang Li, Shubhabrata Mukherjee, et al. Systematic tissue-specific functional annotation of the human genome highlights immune-related DNA elements for late-onset Alzheimer’s disease. *PLoS genetics*, 13(7):e1006933, 2017.
- [24] Qiongshi Lu, Ryan Lee Powles, Qian Wang, Beixin Julie He, and Hongyu Zhao. Integrative tissue-specific functional annotations in the human genome provide novel insights on many complex traits and improve signal prioritization in genome wide association studies. *PLoS genetics*, 12(4):e1005947, 2016.

- [25] Qiongshi Lu, Xinwei Yao, Yiming Hu, and Hongyu Zhao. GenoWAP: GWAS signal prioritization through integrated analysis of genomic functional annotation. *Bioinformatics*, 32(4):542–548, 10 2015.
- [26] Sotiria Manou-Stathopoulou, Felice Rivellese, Daniele Mauro, Katriona Goldmann, Debasish Pyne, Peter Schafer, Michele Bombardieri, Costantino Pitzalis, and Myles Lewis. 235 IKZF1 and IKZF3 inhibition impairs B cell differentiation and modulates gene expression in systemic lupus erythematosus, 2019.
- [27] Matthew T Maurano, Richard Humbert, Eric Rynes, Robert E Thurman, Eric Haugen, Hao Wang, Alex P Reynolds, Richard Sandstrom, Hongzhu Qu, Jennifer Brody, et al. Systematic localization of common disease-associated variation in regulatory DNA. *Science*, 337(6099):1190–1195, 2012.
- [28] Jingsi Ming, Mingwei Dai, Mingxuan Cai, Xiang Wan, Jin Liu, and Can Yang. LSMM: a statistical approach to integrating functional annotations with genome-wide association studies. *Bioinformatics (Oxford, England)*, 34:2788–2796, August 2018.
- [29] Jingsi Ming, Tao Wang, and Can Yang. LPM: a latent probit model to characterize the relationship among complex traits using summary statistics from multiple GWASs and functional annotations. *Bioinformatics*, 12 2019. btz947.
- [30] Michael A Newton, Amine Noueir, Deepayan Sarkar, and Paul Ahlquist. Detecting differential gene expression with a semiparametric hierarchical mixture method. *Biostatistics*, 5(2):155–176, 2004.
- [31] Majid Nikpay, Anuj Goel, Hong-Hee Won, Leanne M Hall, Christina Willenborg, Stavroula Kanoni, Danish Saleheen, Theodosios Kyriakou, Christopher P Nelson, Jemma C Hopewell, et al. A comprehensive 1000 Genomes-based genome-wide association meta-analysis of coronary artery disease. *Nature genetics*, 47(10):1121, 2015.
- [32] Stan Pounds and Stephan W Morris. Estimating the occurrence of false positives and false negatives in microarray studies by approximating and partitioning the empirical distribution of p-values. *Bioinformatics*, 19(10):1236–1242, 2003.
- [33] Alkes L Price, Chris CA Spencer, and Peter Donnelly. Progress and promise in understanding the genetic basis of common diseases. *Proceedings of the Royal Society B: Biological Sciences*, 282(1821):20151684, 2015.
- [34] Paula S Ramos. Unravelling the complex genetic regulation of immune cells. *Nature Reviews Rheumatology*, pp. 1–2, 2020.
- [35] Iñaki Sanz and F Eun-Hyung Lee. B cells as therapeutic targets in SLE. *Nature Reviews Rheumatology*, 6(6):326, 2010.
- [36] Andrew J Schork, Wesley K Thompson, Phillip Pham, Ali Torkamani, J Cooper Roddey, Patrick F Sullivan, John R Kelsoe, Michael C O’Donovan, Helena Furberg, Tobacco, Genetics Consortium, Bipolar Disorder Psychiatric Genomics Consortium, Schizophrenia Psychiatric Genomics Consortium, Nicholas J Schork, Ole A Andreassen, and Anders M Dale. All SNPs are not created equal: genome-wide association studies reveal a consistent pattern of enrichment among functionally annotated SNPs. *PLoS genetics*, 9:e1003449, April 2013.
- [37] Rachel CY Tam, Alfred LH Lee, Wanling Yang, Chak Sing Lau, and Vera SF Chan. Systemic lupus erythematosus patients exhibit reduced expression of CLEC16A isoforms in peripheral leukocytes. *International journal of molecular sciences*, 16(7):14428–14440, 2015.
- [38] The GTEx Consortium. The Genotype-Tissue Expression (GTEx) pilot analysis: Multitissue gene regulation in humans. *Science*, 348(6235):648–660, 2015.

- [39] Rong W Zablocki, Andrew J Schork, Richard A Levine, Ole A Andreassen, Anders M Dale, and Wesley K Thompson. Covariate-modulated local false discovery rate for genome-wide association studies. *Bioinformatics (Oxford, England)*, 30:2098–2104, August 2014.

Supplementary Material for “GPA-Tree: Statistical Approach for Functional-Annotation-Tree-Guided Prioritization of GWAS Results”

1 Details of GPA-Tree

Assuming the SNPs are independent, we can write the joint distribution of the observed data $Pr(\mathbf{Y}, \mathbf{A})$ as shown below.

$$\begin{aligned} P(\mathbf{Y}, \mathbf{A}) &= \prod_{i=1}^M [P(Z_i = 1)P(Y_i; Z_i = 1, A_i.) + (Z_i = 0)P(Y_i; Z_i = 0, A_i.)] \\ &= \prod_{i=1}^M [\pi_i \alpha y_i^{\alpha-1} + (1 - \pi_i)] \end{aligned}$$

The incomplete data log-likelihood (ℓ_{IC}) and the complete data log-likelihood (ℓ_C) for GPA-Tree are also shown below.

$$\begin{aligned} \ell_{IC} &= \sum_{i=1}^M \log [P(Z_i = 1)P(Y_i; Z_i = 1) + P(Z_i = 0)P(Y_i; Z_i = 0)] \\ &= \sum_{i=1}^M \log [\pi_i \alpha y_i^{\alpha-1} + (1 - \pi_i)] \end{aligned}$$

$$\ell_C = \sum_{i=1}^M [Z_i (\log \pi_i + \log \alpha + (\alpha - 1) \log y_i) + (1 - Z_i) \log(1 - \pi_i)]$$

2 Additional Figures

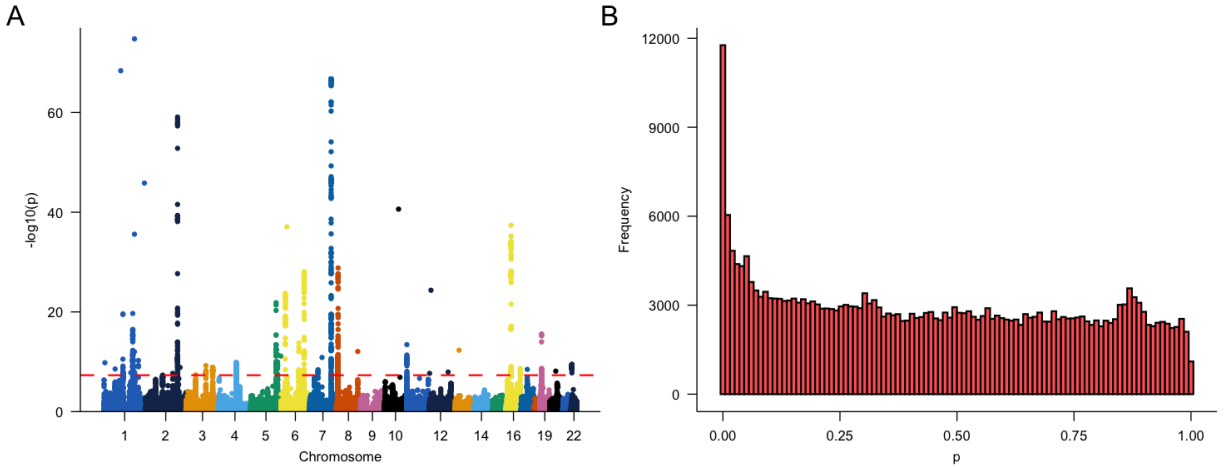


Figure 4: Characteristics of the SLE GWAS data. (A) Manhattan plot. Genome-wide significance level (5×10^{-8}) is indicated by the dashed red line. (B) GWAS association p -value histogram.

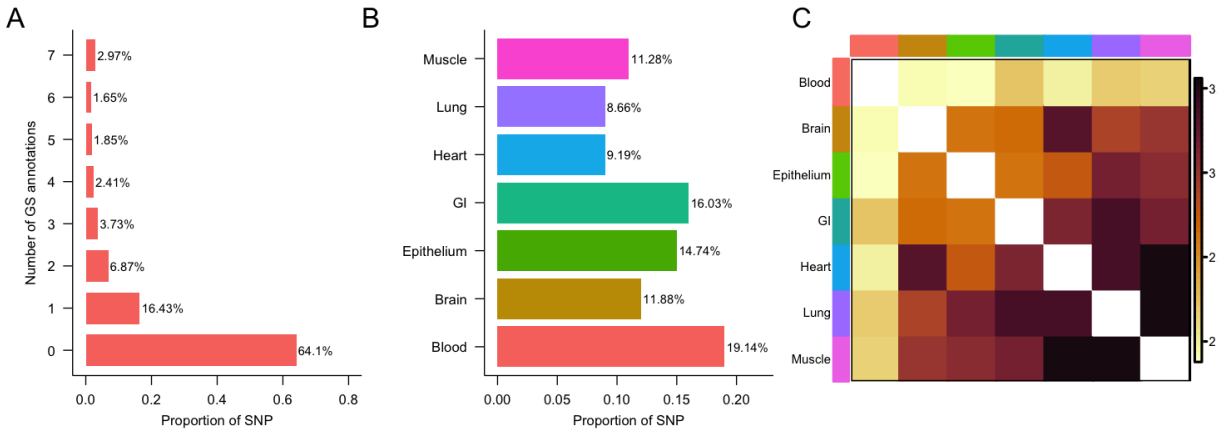


Figure 5: Characteristics of 293,976 SNPs when integrated with seven GenoSkyline (GS) annotations. (A) Number of GS tissues in which SNPs are annotated. (B) Proportion of SNPs that are annotated for each GS tissue type. (C) Overlap of SNPs annotated by seven GS tissue types, calculated using log odds ratio.

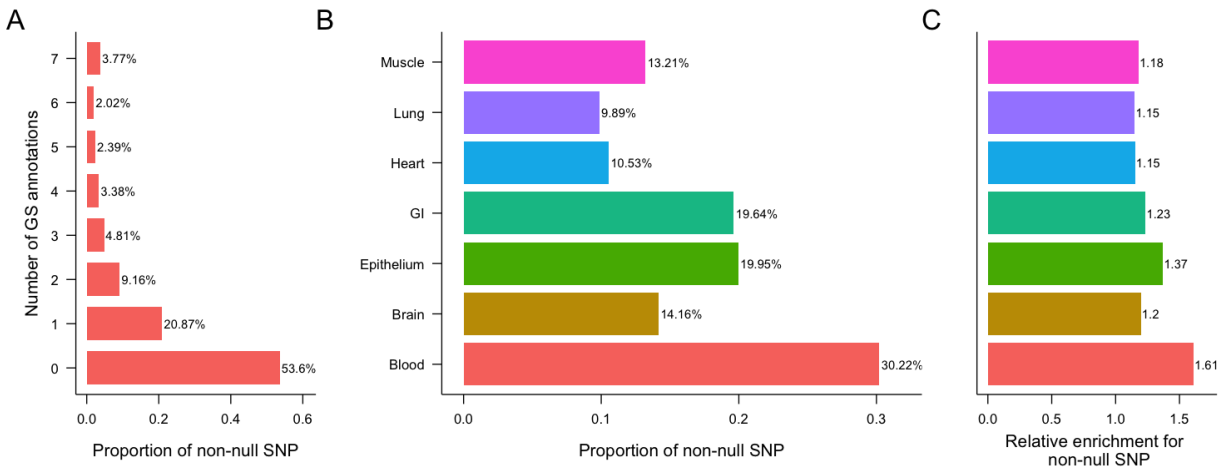


Figure 6: Characteristics of the 8,962 GPA-Tree identified SLE-associated SNPs when integrated with seven GenoSkyline (GS) annotations. (A) Number of GS tissues in which SLE-associated SNPs are annotated. (B) Proportion of SLE-associated SNPs annotated in each GS tissue type. (C) Relative enrichment (RE) of GS tissue types for SLE-associated SNPs. RE is defined as the ratio of the proportion of SLE-associated SNPs that are annotated for a specific GS tissue type, relative to the the proportion of non-SLE-associated SNPs that are annotated for the same GS tissue type.

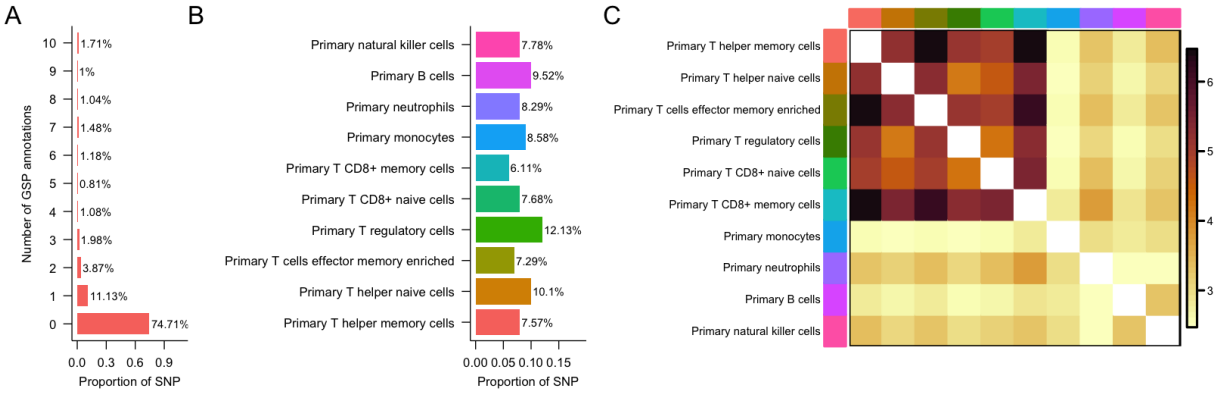


Figure 7: Characteristics of the 293,976 SNPs when integrated with 10 GenoSkylinePlus (GSP) blood-related annotations. (A) Number of blood-related GSP annotation type in which SNPs are annotated. (B) Proportion of SNPs annotated for each blood-related GSP annotation type. (C) Overlap of SNPs annotated by 10 blood-related GSP cell types, calculated using log odds ratio.

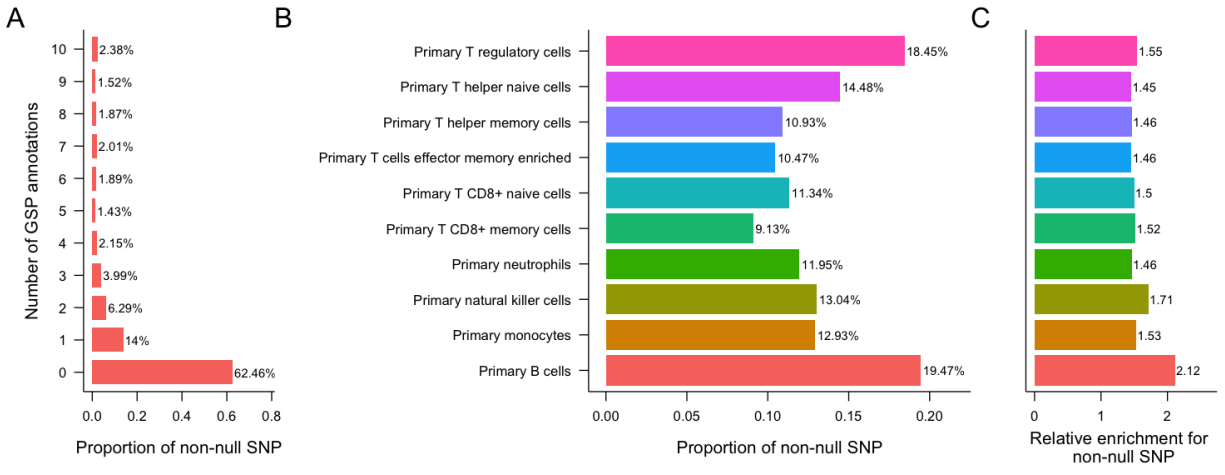


Figure 8: Characteristics of the 8,993 GPA-Tree identified SLE-associated SNPs when integrated with 10 blood-related GSP annotations. (A) Number of blood-related GSP annotations in which SLE-associated SNPs are annotated. (B) Proportion of SLE-associated SNPs annotated in each of the blood-related GSP annotation type. (C) Relative enrichment (RE) of blood-related GSP cell type for SLE-associated SNPs. RE is defined as the ratio of the proportion of SLE-associated SNPs that are annotated for a specific blood-related GSP cell type, relative to the the proportion of non-SLE-associated SNPs that are annotated for the same blood-related GSP cell type.